JOURNAL OF MATERIALS SCIENCE 13 (1978) 2029–2036

Dislocations in neodymium gallium garnet ($Nd_3Ga_5O_{12}$ or NdGG)

J. W. MATTHEWS*, T. S. PLASKETT
IBM Thomas J. Watson Research Center, Yorktown Heights, New York 10598, USA

Dislocations in imperfect (1 1 1) and (1 0 0) wafers of neodymium gallium garnet ($Nd_3 Ga_5 O_{12}$ or NdGG) have been examined using etch pits and the bi-refringence method. Long straight dislocations, large prismatic loops, small prismatic loops, dislocation nodes, and low-angle grain boundaries were observed. The Burgers vectors of some of the dislocations lay along the ⟨1 1 0⟩ or ⟨1 1 1⟩ directions. Dislocations with Burgers vectors along ⟨1 0 0⟩ may have been present, but conclusive evidence for this was not obtained. The diameter of the smallest prismatic loop was 3.1 μm. It is thought to be the smallest dislocation loop observed by the bi-refringence method. The rotation across the low-angle grain boundaries was $\sim 10^{-6}$°.

1. Introduction

Many bubble domain devices are made by depositing magnetic garnet films onto wafers of gadolinium gallium garnet ($Gd_3 Ga_5 O_{12}$ or GGG) [1]. A much smaller number are prepared on wafers of neodymium gallium garnet ($Nd_3 Ga_5 O_{12}$ or NdGG) [2]. However, it is possible that the use of NdGG will increase. Advantages of NdGG are (a) that it has a relatively low melting point [3] and is easier to grow than GGG, and (b) that its lattice parameter matches those of garnets which are able to provide minimally small magnetic bubble domains [2].

A crucial factor in the performance of devices prepared on GGG or NdGG wafers is the dislocation content of the films. Dislocations are important because they impede bubble motion [4]. Etch pits [5], X-ray topographs [6], and bi-refringence images [7] of dislocations have revealed that the majority of dislocations in films are simply extensions of those that terminated on the substrate surface before film growth began. Thus, the elimination of dislocations from garnet films must begin with the preparation of dislocation-free substrate wafers. This, in turn, requires that dislocation-free boules be grown. Advances in crystal growth have led to routine production of GGG crystals that are free or almost free of dislocation lines. Dislocation-free crystals of NdGG have been grown but not routinely.

The similarities of GGG and NdGG suggest that similar dislocations will be found in them. To test this we have examined dislocations in NdGG wafers using the etch pit method, and stress induced bi-refringence. The bi-refringence technique was discovered by Bond and Andrus [8] and first applied to a garnet ($Y_3 Ga_5 O_{12}$ or YGG) by Prescott and Basterfield [9]. This early work was followed by many investigations of GGG using the bi-refringence method [10–13]. The results were consistent with Prescott and Basterfield's observations, and with other studies of GGG made using X-ray topography [14]. The optical images of dislocations in GGG also revealed that stress-induced bi-refringence is more versatile than had been realized. The images demonstrated that dislocations did not need to be along the optical axis of the microscope in order to be seen [10–13, 15]. They also showed that the method could be applied to very large crystals [16]. The only other non-destructive technique that can be used to examine dislocations in crystals that are thick as well as large in lateral extent seems to be neutron topography [17].

*Deceased, May 15, 1977.

2. Experimental details

Large NdGG crystals were grown from iridium crucibles by the Czochralski technique and cut into wafers ~ 0.5 mm in thickness. The surfaces of the wafers were parallel to the (1 1 1) or (1 0 0) planes. Some wafers were etched in a mixture of concentrated sulphuric and phosphoric acid to form pits where dislocation lines terminated on the sample surface. All wafers were examined in a polarizing microscope, with polarizer and analyser set at right angles. The wafers selected for detailed examination were much less perfect than average: they contained about 10^4 dislocations cm^{-2}.

3. Observations

3.1. Threading dislocations

Examples of dislocations with lines that extended from one surface of a (1 1 1) wafer to the other are seen in Fig. 1. This figure contains six of the same area. The microscope was focused on

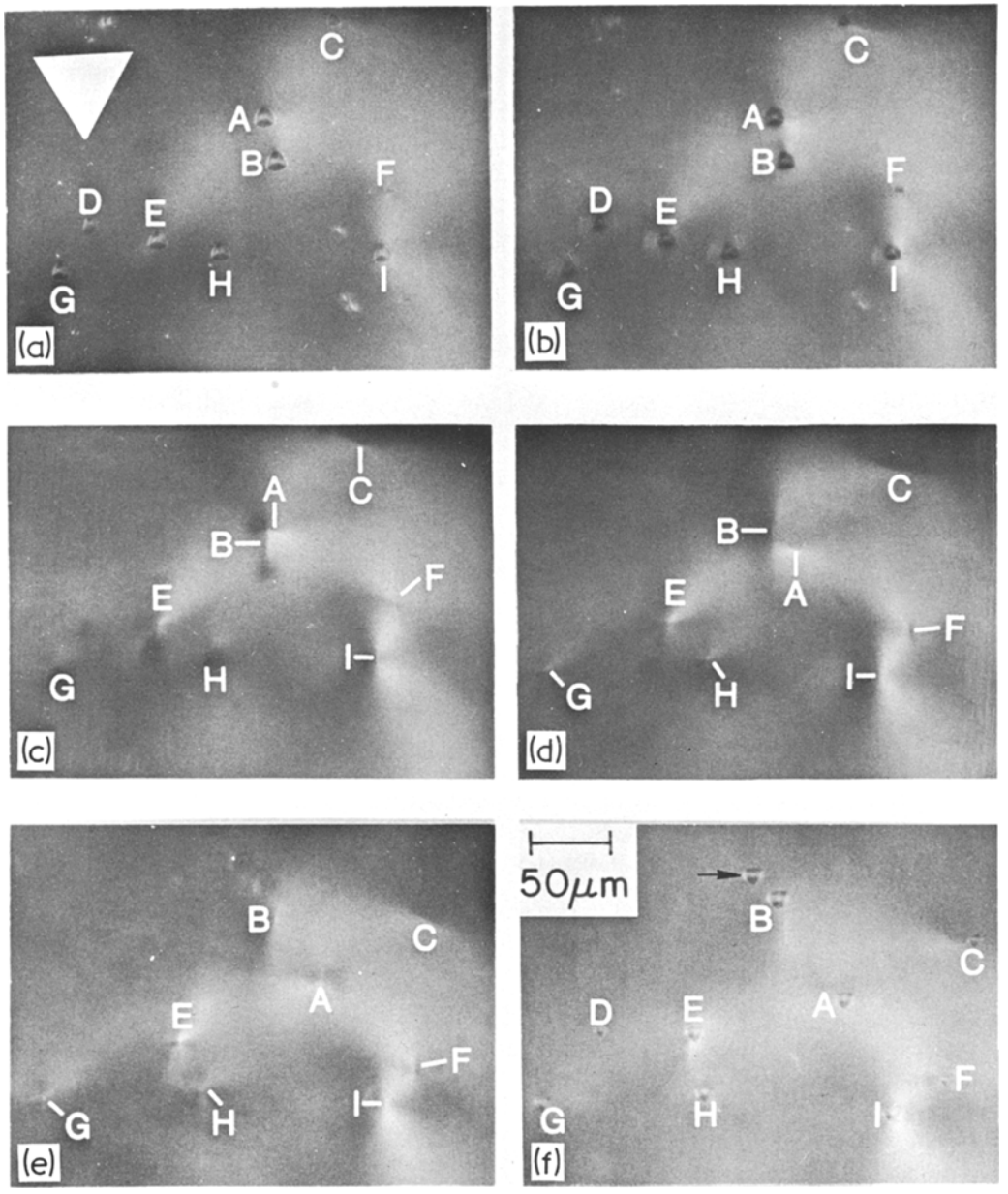

Figure 1 Micrographs at different focal settings of dislocations in a (1 1 1) wafer of NdGG. The edges of the white triangle in (a) are parallel to the ⟨1 1 0⟩ directions in the wafer plane. Polarizer and analyser are inclined at 45° to the borders of the figure.

the lower surface in (a) and on the upper one in (f). Triangular etch pits are visible in (a) and (f), and bi-refringence images of the dislocations can be seen in the remainder. Dislocations labelled A and B cross one another on their way through the crystal: A is above B in (a) and below (b) in F. This would have been difficult to deduce from the images of the etch pits alone.

Dislocation C appears to go through the sample at an oblique angle. However, measurements show that it is inclined at $\sim 12^{\circ}$ to the normal to the wafer plane. The illusion that it is more obliquely inclined than this results from the high refractive index of NdGG.

Etch pits labelled D can be seen in (a), (b) and (f). However, these pits differ from the others present in that no bi-refringence image is associated with them. This, taken together with the fact that D in (a) lies almost vertically above D in (f), suggests that the dislocation responsible for D was in screw orientation [15, 18–20]. If this is so then the Burgers vector of D was along [1 1 1].

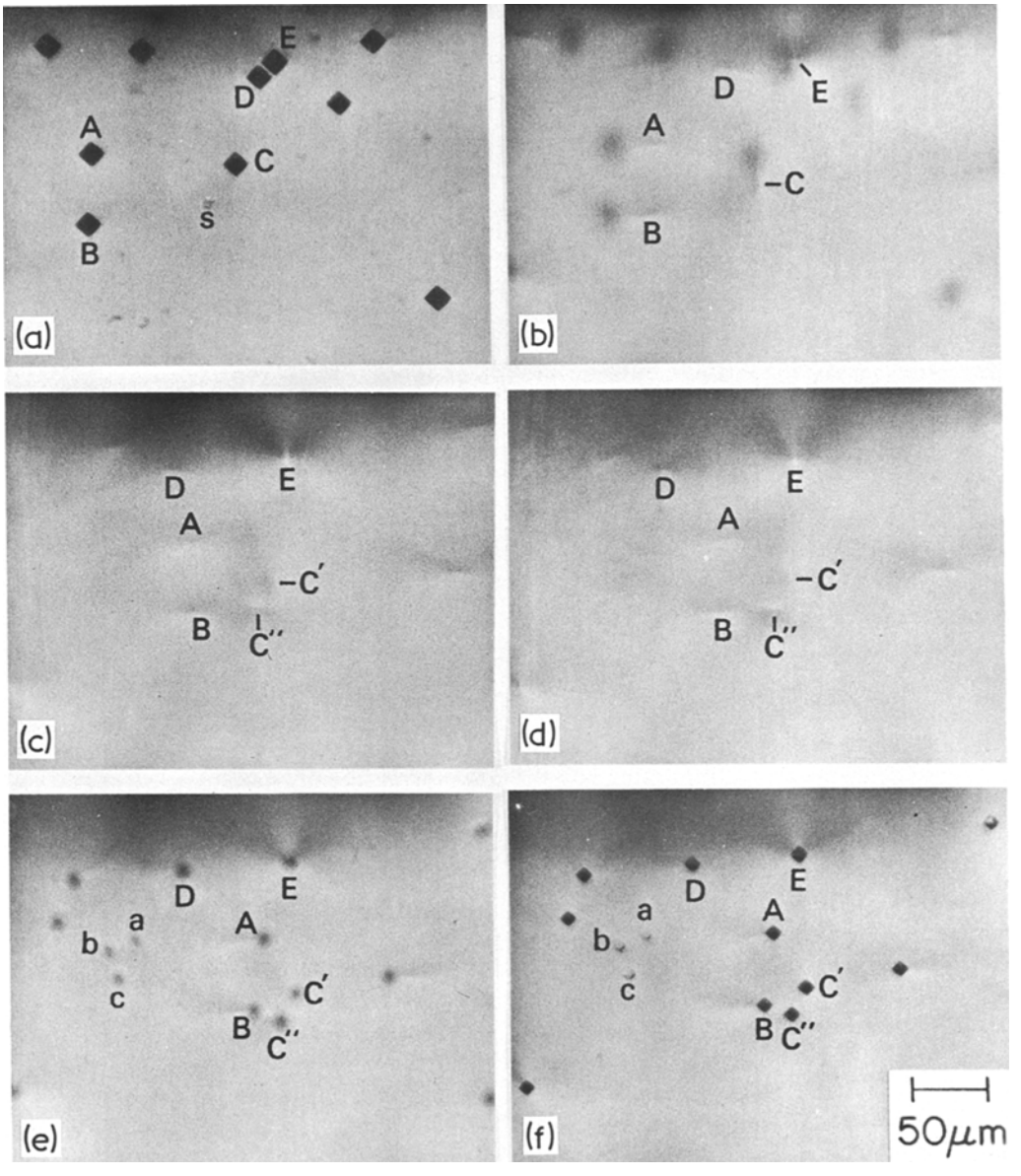

Figure 2 Micrographs at different focal settings of an (0 0 1) wafer of NdGG. (a) shows the lower surface of the wafer and (f) the upper. The edges of the etch pits are parallel to ⟨1 0 0⟩ directions in the wafer plane. Polarizer and analyser were inclined at 45° to the border of the figure.

The images of E, F, G, H and I show that their lines were inclined at $\lesssim 7°$ to the normal to the wafer plane. As the plane of the wafer in Fig. 1 was perpendicular to the growth direction this result means that many dislocation lines were approximately but not precisely parallel to the growth axis. Similar results have been obtained for GGG by Glass [20]. The images of E and I suggest that the edge components of their Burgers vectors (projected into the film plane) lay along ⟨1 1 2⟩. If we assume this result, and, in addition, assume that the Burgers vectors of dislocations in garnets lie along the ⟨1 1 1⟩, ⟨1 1 0⟩ or ⟨1 0 0⟩ directions, then the Burgers vectors of E and I were probably parallel to ⟨1 1 1⟩. However, it is also possible that their Burgers vectors were along ⟨1 1 0⟩.

Fig. 2 is a series of micrographs of a portion of an etched (1 0 0) wafer. Micrograph (a) is the lower surface and (f) the upper. The edges of the pits in (a) and (f) lie along the ⟨0 0 1⟩ directions in the (1 0 0) plane. Dislocations labelled A and B move from left to right as one goes from (a) to (f). D, on the other hand, moves from right to left. The inclination of A and B to the normal to the sample plane was about 15°.

Pit C in Fig. 2a is associated with a single bi-refringence image in (b). However, between (b) and (c) the bi-refringence image changes from that of a single dislocation into that of a pair of dislocations labelled C′ and C″. C′ and C″ move further apart between (c) and (d) and give rise to a pair of clearly resolved pits in (f). The dissociation of C into C′ and C″ means that there was a dislocation node in Fig. 2. Dislocation nodes have been found in GGG but were rare [16].

The contrast at E in Figs. 2c and d suggests that the edge component of E (projected into the film plane) was parallel to the horizontal border of the figure. This in turn suggests that the Burgers vector of B was parallel to [1 1 0], possibly, or [1 1 1].

A feature of Figs. 2e and f is the presence of three small pits labelled a, b and c. These pits are unlike those associated with threading dislocations and there is no discernible bi-refringence associated with them. Also they do not have counterparts in Fig. 2a. (The feature labelled s in (a) is a scar on the sample surface and not the image of an etch pit). The origin of a, b and c in Fig. 2f has not been determined. However, observations on GGG [21] suggest that they may have been caused by small precipitate particles.

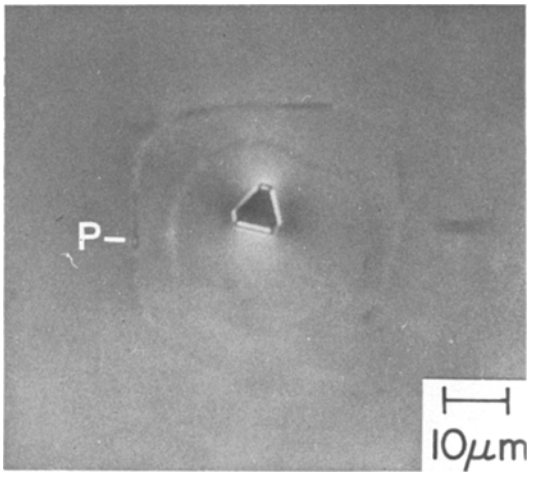

Figure 3 A pair of prismatic loops around an iridium inclusion in a (1 1 1) wafer. P is a precipitate particle formed along the dislocation line. Polarizer and analyser were inclined at 45° to the borders of the figure.

3.2. Dislocation loops

3.2.1. Loops around precipitates or inclusions

Fig. 3 shows a pair of dislocation loops that encircle an iridium inclusion in a (1 1 1) wafer. The plane of the loops is (1 1 1), and the loops themselves go out of contrast when the polarizer or analyser is parallel to their line. These features suggest [15, 22] that the loops were prismatic and that their Burgers vectors were parallel to [1 1 1]. Prismatic loops that encircled iridium inclusions and had Burgers vectors along ⟨1 1 1⟩ have been observed in GGG [10].

A feature of the loops in Fig. 3 is the presence of precipitate particles, like P, along them. Precipitates have recently been observed at loops in GGG [21]. However, the prismatic loops in the early GGG crystals [10] did not have discernible precipitates associated with them.

Fig. 4 shows a pair of loops L_1 and L_2 around a small dark particle in an (0 0 1) wafer. The inclination of the loops to the wafer surface, and the fact that they lie on a plane which intersects (0 0 1) along [1 0 0], shows that they were approximately parallel to the (0 1 1) plane. Comparison of the loops in Fig. 4 with the (0 1 1) loops found in GGG [10] suggests that the loops in Fig. 4 were prismatic and that their Burgers vectors were parallel to [0 1 1].

The feature labelled I in Fig. 4 is an out of focus image of an iridium inclusion. The compo-

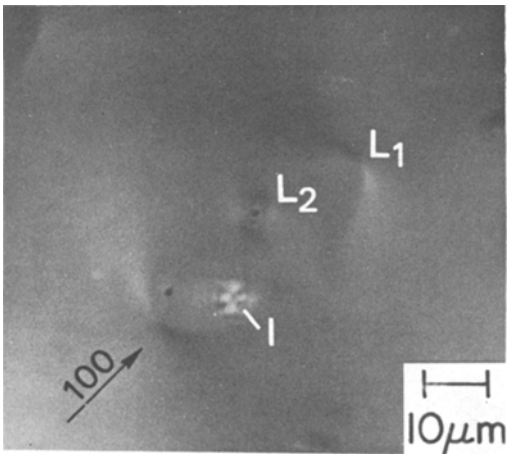

Figure 4 A pair of dislocation loops, $L_{1,2}$ in a (1 0 0) wafer of NdGG. The portions of L_1 that are imagined in sharp focus, and the inclination of L_1 to the wafer plane, show that it was parallel to {1 1 0}. Polarizer and analyser were inclined at 45° to the border of the figure.

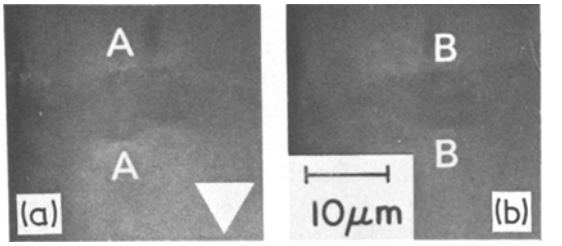

Figure 5 A pair of small prismatic loops, A and B, in a (1 1 1) wafer. The ⟨1 1 0⟩ directions in (1 1 1) are given by the edges of the white triangle. The two micrographs are of the same specimen area. Loop A is imaged in sharp focus in (a) and B is in sharp focus in (b). Polarizer and analyser were inclined at 45° to the borders of the figure.

sition of the two dark dots inside L_1 and L_2 is not known.

Although the loops in Figs. 3 and 4 are amongst the largest found in NdGG, and are much larger than those commonly found in crystals, they are smaller than those observed in GGG [10, 14]. The largest loops in GGG were about ten times the diameter of those in Figs. 3 and 4.

3.2.2. Small loops on {1 1 0}

High magnification images of NdGG crystals revealed many prismatic loops significantly smaller than those described in Section 3.2.1. The loops lay on {1 1 0} planes and did not have visible precipitates at their centres. However, it should be emphasized that it is possible that precipitates were present but did not absorb or scatter sufficient light to be seen.

Examples of the small loops are labelled A and B in Fig. 5. The loops in Fig. 5 lie on a {1 1 0} plane perpendicular to the film plane. Their images are the same as those expected from pairs of edge dislocations of opposite sign [18, 19, 23]. The orientation of the edge dislocations were such that Burgers vectors of the dislocations were perpendicular to the line joining them.

Evidence that the pairs of dislocations in Fig. 5 were the opposite sides of loops, and not threading dislocations of opposite sign, is provided by the fact that the dislocations were clearly visible at only one setting of the microscope. If the microscope was either raised or lowered the dislocation contrast gradually disappeared. This is demonstrated by the two parts of Fig. 5. The microscope was raised 6 μm between the recording of (a) and (b). The dislocations labelled A are sharply imaged in (a) but not in (b). Those labelled B are sharply imaged in (b) but not in (a).

The diameters of the loops in Fig. 5 were 8.5 and 7.2 μm. The smallest loop we have seen was 3.1 μm in diameter. This seems to be the smallest loop that has been observed by stress-induced birefringence. It is of some interest to compare its diameter with the diameters of loops observed by other methods. Rabier *et al.* [24] have observed loops in yttrium iron garnet using transmission electron microscopy. The largest loop they found was about one sixth of the diameter of the smallest loop that we have seen. The smallest loops detected by X-ray topography [25, 26] are much larger than the smallest loops that we have seen. The smallest loop that could be observed by the decoration method [27] is fixed by the resolution unit limit of the light microscope. It is thus about one tenth of the diameter of the smallest loop observed in NdGG.

3.3. Burgers vectors of dislocations

The results in Sections 3.1 and 3.2 indicate that dislocations with Burgers vectors along ⟨1 1 0⟩ and ⟨1 1 1⟩ were present in NdGG. However, the results in these sections do not provide evidence for dislocations with Burgers vectors along ⟨1 0 0⟩. The purpose of this section is to point out that, although we do not have compelling evidence for Burgers vectors along ⟨1 0 0⟩, we have made many observations that are consistent with the presence of dislocations with Burgers vectors along ⟨1 0 0⟩.

Fig. 6a shows a portion of the surface of an etched (1 0 0) wafer. Fig. 6b is a bi-refringence image of the dislocation in the interior of the sample. The images of the four dislocations near the centre of Fig. 6 show that their lines were almost parallel to the optical axis, that they had large edge components, and that the projections of these components lay along the [1 0 0] direction in the (0 0 1) wafer plane. If we assume [9, 10] that the dislocations in garnets have Burgers vectors along ⟨1 1 1⟩, ⟨1 1 0⟩ or ⟨1 0 0⟩, then the Burgers vectors of the dislocations near the centre of Fig. 6 lie along [1 0 0] or [1 0 1].

3.4. Absence of helical dislocations

Imperfect GGG crystals contained unusually large helical dislocations [6, 11]. Helical dislocations have not been found in NdGG crystals.

3.5. Low-angle grain boundaries

Imperfect NdGG crystals contained a number of very low-angle grain boundaries. The boundaries resembled those in GGG [5] in that their structure varied greatly along their length. Some parts of the boundaries consisted of regularly spaced parallel dislocations. Other parts were made up of rather irregularly arranged dislocation lines. The boundary in Fig. 7 consists of regularly arranged dislocations near A and rather irregularly arranged ones elsewhere. The pairs of dislocations labelled a, b and c resemble the paired dislocations found in grain boundaries in germanium and silicon crystals by Oberly [28] and Okada [29].

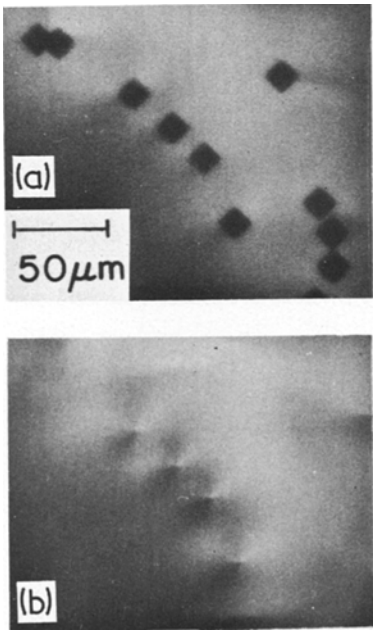

Figure 6 Micrographs of the surface and interior of an (0 0 1) wafer. The image contrast of the four dislocations near the centre of the figure is consistent with their having Burgers vectors whose edge components in the wafer plane are parallel to [1 0 0]. Polarizer and analyser were at 45° to the borders of the figure.

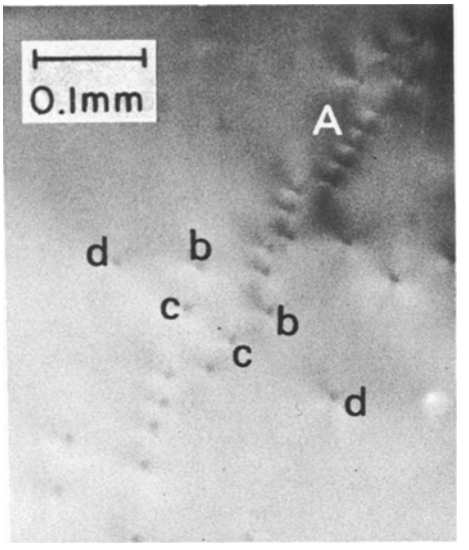

Figure 7 A low-angle grain boundary in an (0 0 1) wafer of NdGG. The dislocations are arranged in a parallel uniformly spaced array near A, but are less regularly arranged elsewhere. Polarizer and analyser were inclined at 45° to the borders of the figure.

A portion of a grain boundary in which the arrangement of dislocations is different from that usually assumed for low-angle boundaries, and different from the less regular arrangements studied by Oberly and Okada, is seen in Fig. 8. The boundary in this figure consists of two almost parallel columns, x and y, of dislocations which have large edge components and lines approximately parallel to the optic axis. The image contrast at the dislocations shows that they were all of the same size [10, 15, 23] and that their Burgers vector [18] projected into the wafer plane lay along [1 1 0]. A feature of x and y is that the dislocations in y fall into the gaps between the dislocations in x. This holds even when there is a dislocation missing from x or y. Similar arrangements of edge dislocations have been observed in crystals of GGG (see Figs. 10b and 11 of [10]). If we assume that the Burgers vectors of the dislocations in Fig. 8 were along [1 1 0], then the rotation across the boundary was $\sim 10^{-6}$°.

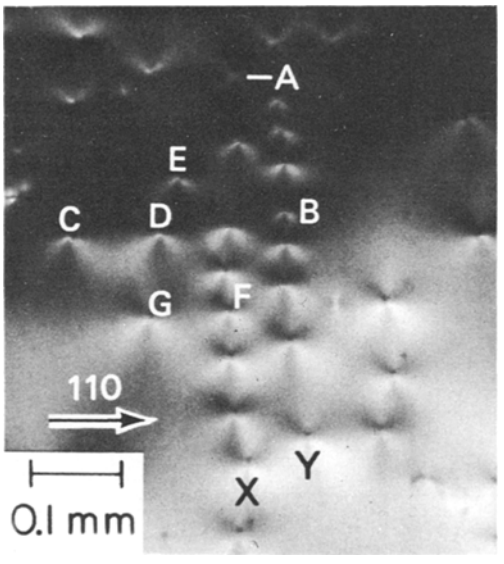

Figure 8 A portion of a low-angle boundary in an (0 0 1) wafer of NdGG. Polarizer and analyser were at 45° to the borders of the figure. The rotation across the boundary was about 10^{-6} degrees. The length of the scale marker is approximately equal to the resolution limit of the eye.

3.6. Two features of bi-refringence images of dislocations

Two features of bi-refringence images of dislocations are shown by Fig. 8. The first is that the size of the image of a dislocation depends upon the distance between the dislocation and its neighbours. For example, the image of the rather isolated dislocation labelled G is larger than the image of F which has a number of near neighbours. Also, the images of dislocations C and D are larger than the image of B. The explanation for this pheonomenon is that the bi-refringence image of a dislocation occupies the region where the dislocation's elastic strain field dominates over the strain fields of the other dislocations present. This feature of bi-refringence images has some practical importance. If the dislocation density in a crystal is low the images of individual dislocations are larger and low magnification images can be used to observe them. On the other hand, if the dislocation density is high the images are small and closely spaced dislocations can be resolved. The dislocation density at which individual dislocations become difficult to observe by the bi-refringence method is not known. However, the observation of a loop $\sim 3\,\mu m$ in diameter suggests that it is about $10^7\,cm^{-2}$.

The second feature shown by Fig. 8 is that dislocations are easy to observe if the background contrast is grey, but are rather difficult to detect if the background is black. This can be seen by comparing the image of dislocation A with the images of the dislocations in the lower portion of the figure. The visibility of A becomes comparable with that of the dislocations in the lower half of the figure if the exposure is increased by a factor of five or ten.

Black backgrounds to dislocations are obtained when the medium surrounding the dislocations is either unstressed or stressed in such a way as not to change the polarization of the incident light beam. Grey backgrounds (and dark and light lobes in the dislocation images) result from long layer stresses that do change the polarization of the incident light beam [10, 15, 23].

4. Conclusions

Imperfect NdGG crystals have been found to contain long straight dislocations, large straight dislocations, large prismatic loops, small prismatic loops, dislocation nodes, and grain boundaries of very low angle. The large prismatic loops encircled iridium inclusions, or unidentified precipitate particles, and often had precipitate particles found along them. The small loops did not have visible precipitates or inclusions associated with them. They are thought to be the smallest loops that have been observed by the bi-refringence method.

Some dislocations had Burgers vectors along ⟨1 1 1⟩. Others had Burgers vectors along ⟨1 1 0⟩. Dislocations with Burgers vectors along ⟨1 0 0⟩ may have been present but we do not have conclusive evidence for this.

Bi-refringence images of dislocations are larger when the dislocation density is low but small when their density is high. Thus, low magnification images can be used to examine the dislocations in large, almost perfect, crystals. High magnification images can be used to observe individual dislocations in crystals that may contain as many as $\sim 10^7$ dislocations per cm^2.

Acknowledgements

The technical assistance of A. H. Parsons and J. M. Karasinski and the helpful discussions of Dr P. Chaudhari are appreciated. This research was partially supported by the Air Force Office of Scientific Research under contract number F49620-77-C-0060.

References

1. A. H. BOBECK and E. DELLA TORRE, "Magnetic Bubbles" (North Holland, Amsterdam, 1975) p. 114.
2. T. S. PLASKETT, E. KLOKHOLM, D. C. CRONEMEYER, P. C. YIN and S. E. BLUM, *Appl. Phys. Lett.* **25** (1974) 357.
3. C. D. BRANDLE and A. J. VALENTINO, *J. Cryst. Growth* **12** (1972) 3.
4. B. E. ARGYLE and P. CHAUDHARI, *AIP Conf., Proc.* **10** (1973) 403.
5. D. C. MILLER, *J. Electrochem Soc.* **120** (1973) 678.
6. W. T. STACEY, J. A. PISTORIUS and M. M. JANSEN, *J. Cryst. Growth* **22** (1974) 37.
7. J. W. MATTHEWS, E. KLOKHOM and T. S. PLASKETT, *AIP Conf. Proc.* **10** (1973) 271.
8. W. L. BOND and J. ANDRUS, *Phys. Rev.* **101** (1956) 1211.
9. M. J. PRESCOTT and J. BASTERFIELD, *J. Mater. Sci.* **2** (1967) 583.
10. J. W. MATTHEWS, E. KLOKHOLM, V. SADAGOPAN, T. S. PLASKETT and E. MENDEL, *Acta Met.* **21** (1973) 203.
11. J. W. MATTHEWS, E. KLOKHOLM, T. S. PLASKETT and V. SADAGOPAN, *Phys. Stat. Sol. (a)* **19** (1973) 671.
12. J. W. MATTHEWS, E. KLOKHOLM and T. S. PLASKETT, *IBM J. Res Develop.* **17** (1973) 426.
13. B. COCKAYNE and J. M ROSINGTON, *J. Mater. Sci.* **8** (1973) 601.
14. K. LAE and S. MADER, *J. Cryst. Growth* **22** (1974) 37.
15. B. K. TANNER and D. J. FATHERS, *Phil. Mag.* **29** (1974) 1081.
16. J. W. MATTHEWS, T. S. PLASKETT and J. AHN, *ibid.* **33** (1976) 73.
17. C. MALGRANGE, J. F. PETROFF, M. SAVAGE and A. ZARKA, *ibid.* **33** (1976) 743.
18. R. BULLOUGH, *Phys. Rev.* **110** (1958) 620.
19. V. L. INDENBOM and G. E. TOMILOVSKII, *Soviet Phys., Crystallogr.* **2** (1957) 183.
20. H. L. GLASS, *Mater. Res. Bull.* **8** (1973) 43.
21. J. W. MATTHEWS and T. S. PLASKETT, *Phys. Stat. Sol. (a)* **38** (1976) 577.
22. *Idem ibid.* **37** (1976) 499.
23. D. A. JENKINS and J. J. HREN, *Phil. Mag.* **33** (1976) 173.
24. J. RABIER, H. GAIEM and P. VEYSSIÈRE, *J. Appl. Phys.* **47** (1976) 4755.
25. J. R. PATEL, *ibid.* **44** (1973) 3903.
26. J. R. PATEL and A. AUTHIER, *ibid.* **46** (1975) 118.
27. J. M. HEDGES and J. W. MITCHELL, *Phil. Mag.* **44** (1953) 223.
28. J. J. OBERLY, *J. Metals* **6** (1954) 1205.
29. K. OKADA, *J. Phys. Soc. Japan* **10** (1955) 1018.

Received 3 January and accepted 31 January 1978.